ARTICLE

BIOTECHNOLOGY and BIOENGINEERING

Selective Bioparticle Retention and Characterization in a Chip-Integrated Confocal Ultrasonic Cavity

J. Svennebring,[1] O. Manneberg,[1] P. Skafte-Pedersen,[2] H. Bruus,[2] M. Wiklund[1]

[1]Biomedical & X-Ray Physics, Department of Applied Physics, Royal Institute of Technology, SE-106 91 Stockholm, Sweden; telephone: +46-8-5537-8134; fax: +46-8-5537-8466; e-mail: martin@biox.kth.se

[2]Department of Micro- and Nanotechnology, Technical University of Denmark, Kongens Lyngby, Denmark

Received 3 August 2008; revision received 2 November 2008; accepted 30 December 2008

Published online 6 January 2009 in Wiley InterScience (www.interscience.wiley.com). DOI 10.1002/bit.22255

ABSTRACT: We demonstrate selective retention and positioning of cells or other bioparticles by ultrasonic manipulation in a microfluidic expansion chamber during microfluidic perfusion. The chamber is designed as a confocal ultrasonic resonator for maximum confinement of the ultrasonic force field at the chamber center, where the cells are trapped. We investigate the resonant modes in the expansion chamber and its connecting inlet channel by theoretical modeling and experimental verification during no-flow conditions. Furthermore, by triple-frequency ultrasonic actuation during continuous microfluidic sample feeding, a set of several manipulation functions performed in series is demonstrated: sample bypass—injection—aggregation and retention—positioning. Finally, we demonstrate transillumination microscopy imaging of ultrasonically trapped COS-7 cell aggregates.

Biotechnol. Bioeng. 2009;103: 323–328.

KEYWORDS: ultrasonic manipulation; cell characterization; microfluidic chip

Introduction

Ultrasonic manipulation technology has recently emerged as a powerful tool for handling micrometer-sized biomaterials (such as cells and bio-functionalized beads) in microfluidic chips (Laurell et al., 2007; Wiklund and Hertz, 2006a), with application examples such as separation and fractionation (Harris et al., 2003; Nilsson et al., 2004; Petersson et al., 2007), washing (Hawkes et al., 2004; Petersson et al., 2005), positioning (Haake et al., 2005), and aggregation and retention (Evander et al., 2007; Hultström et al., 2007; Lilliehorn et al., 2005). Although efficient and compatible with high-throughput operation, the current ultrasonic manipulation technology in chips is typically limited to perform a single manipulation function, which is most often distributed along the whole microchannel. However, Manneberg et al. (2009) have recently demonstrated how to spatially separate and localize several independently addressable manipulation functions in series by geometrically varying the ultrasonic resonance conditions along the microchannel. In the present study, we extend this concept by introducing a chip-integrated confocal ultrasonic cavity designed for selective bioparticle retention and characterization.

Resonant ultrasonic actuation of a microchannel of constant cross-section typically results in transverse acoustic radiation forces (see Fig. 1) that focus the particles in well-defined separated bands along the channel. Favorable acoustic resonance conditions occur when actuating chips of small channel heights at frequencies close to those being multiples of half the acoustic wavelength across the channel width (Hagsäter et al., 2008; Manneberg et al., 2008a). For trapping and retention purposes, however, axial gradients (see Fig. 1b) in the sound field are needed. Such gradients create axial acoustic radiation forces capable of balancing the viscous drag from the fluid flow. Suggested approaches in chips for axial confinement and localization of the ultrasonic forces are based on either confinement of the channel resonance conditions via variations of the channel geometry (Hagsäter et al., 2007; Manneberg et al., 2008b), or confinement of the incident acoustic field via near-field effects from the transducer (Hultström et al., 2007; Lilliehorn et al.,

Correspondence to: M. Wiklund

Contract grant sponsor: 6th Framework Program of the European Community
Contract grant number: NMP4-CT-2004-500039
Contract grant sponsor: Swedish Research Council for Engineering Sciences
Contract grant sponsor: Göran Gustavsson Foundation

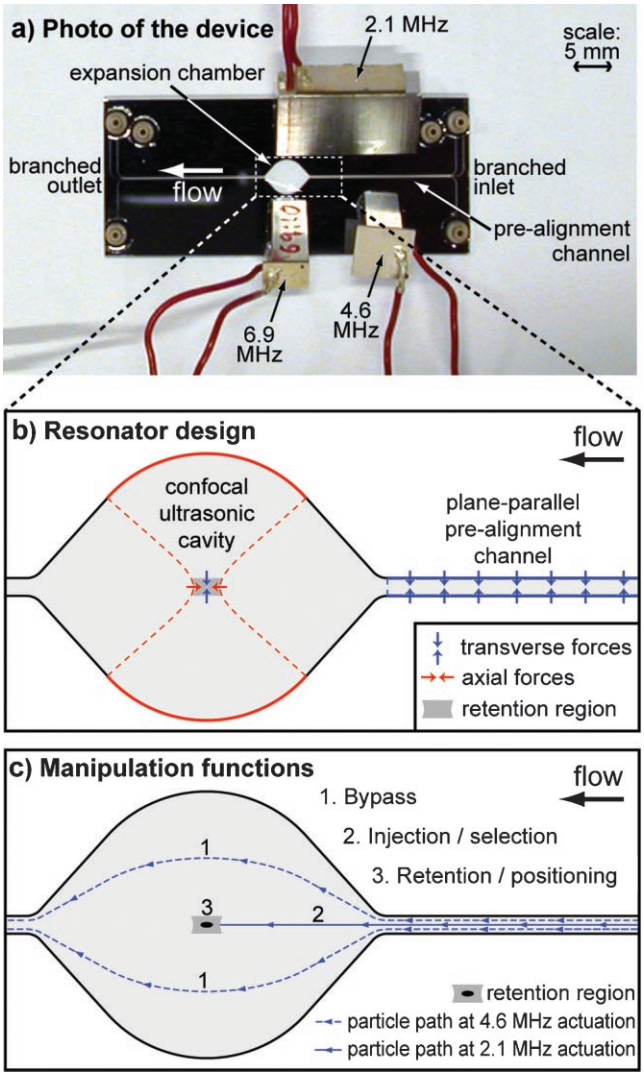

Figure 1. **a**: Photograph of the transducer-chip system. **b**: Illustration of the resonator design: the confocal ultrasonic cavity (in red), and the plane-parallel pre-alignment channel (in blue). The red and blue solid lines indicate the primary reflecting walls of the resonators. The red and blue dashed lines indicate the approximate boundaries of the generated force fields. **c**: Schematic of the available manipulation functions during sample flow: (1) bypass, (2) injection/selection, (3) retention/positioning. The particle paths are defined by the pressure nodes in the pre-alignment channel.

2004). The latter method has been used for sequential trapping of beads above three channel-integrated ultrasonic transducers (Lilliehorn et al., 2005). However, current ultrasonic retention devices cannot be used for the selection of a discrete subpopulation from a continuous sample flow.

Confocal or hemispherical ultrasonic cavities are focused standing-wave resonators based on curved reflector elements. Such resonator designs have previously been employed in macro-scale systems for trapping of millimeter size objects in air (Brandt, 1989; Xie and Wei, 2001), and of micrometer size objects in fluid suspensions (Hertz, 1995; Wiklund et al., 2001, 2004). The curved reflector elements create a focused resonant acoustic field with a highly confined force field, which makes it possible to accurately position objects three-dimensionally (3D) (Hertz, 1995). However, confocal ultrasonic cavities have not yet been investigated in microfluidic chips.

In the present study, we demonstrate and investigate an integrated confocal ultrasonic cavity in a microfluidic chip for selective retention and optical characterization of cells or other bioparticles (Fig. 1). The ultrasound is coupled to the chip by external wedge transducers (Manneberg et al., 2008a; Wiklund et al., 2006b) that are fully compatible with any kind of high-resolution optical microscopy (Manneberg et al., 2008b). In the present work, we investigate the resonant modes in the confocal cavity by theoretical modeling and experimental verification during no-flow conditions. Furthermore, we demonstrate the flow-through operational modes (the manipulation functions) of our device based on triple-transducer actuation, which are (1) pre-alignment and bypassing of cells, (2) selective injection of cell by pre-alignment frequency shift, (3) trapping, retention, and positioning of cells in the center of the expansion chamber, and finally (4) label-free transillumination optical microscopy of a monolayer aggregate of retained cells. The purpose of our design is to select, retain, and position a discrete subpopulation of up to ~100 cells from a continuous feeding sample flow for dynamic optical characterization.

Device

The device (Fig. 1a) consists of a dry-etched silicon structure sandwiched between two glass layers (GeSim, Dresden, Germany), and three external transducers with refractive elements (Manneberg et al., 2008a) placed on top of the chip for efficient coupling of ultrasound into the channel. The layer dimensions of the chip were 200/110/1,100 μm (bottom glass, silicon, upper glass), respectively. The resonator elements are illustrated in Figure 1b. The 328 μm wide inlet channel was used as a plane-parallel resonator (indicated with blue solid lines in Fig. 1b) for particle pre-alignment, bypassing and selection, and was operated in either dual-node (at 4.6 MHz) or single-node (at 2.1 MHz) mode (see blue dashed and solid lines, respectively, in Fig. 1c). The expansion chamber, intended for sample retention and positioning, was designed as a resonant confocal cavity with two cylindrical segments separated by twice their radius of curvature $2R = 4.92$ mm (indicated with red solid lines in Fig. 1b), for maximum axial focusing of the standing wave (indicated with red dashed lines in Fig. 1b). The chamber width was chosen as 15× the width of the pre-alignment channel, which results in approximately the same factor of reduction in the viscous drag on a trapped particle without reducing the flow rate. The chamber was actuated at a frequency close to 6.9 MHz, which also matched with a half wavelength along the channel height for vertical centering (levitation) in the whole chip at this frequency. All actuation voltages were 10 V_{pp}.

The endpoints of the main channel were branched into three inlets and three outlets (see Fig. 1a), although only one inlet and one outlet were used in this work. The flow rate in the chip was controlled by a syringe pump. The chip-transducer system was mounted on an inverted microscope (Axiovert 135; Zeiss, Jena, Germany) for optical monitoring of manipulated particles or cells. Due to the thin bottom glass (200 μm), the fully transparent chip is compatible with both fluorescence (cf. Manneberg et al., 2008b) and transillumination high-resolution optical microscopy (shown in Fig. 5). Five micrometer non-fluorescent polyamide beads (Danish Phantom Design, Jyllinge, Denmark) were used to visualize the acoustic force fields in the expansion chamber, and 10 μm green-fluorescent polystyrene beads (Bangs Laboratories, Fishers, IN) were used as a cell model (i.e., having similar size and acoustic properties) in the experiments simulating manipulation of cells. Finally, COS-7 cells derived from fetal monkey kidney were cultivated and prepared according to the procedure described in Hultström et al. (2007). The cells were used for demonstrating label-free transillumination imaging techniques of a retained cell aggregate.

Simulations

Two-dimensional (2D) simulations of the acoustic pressure field for determination of the eigenmodes and eigenfrequencies were made using the COMSOL eigenvalue solver searching for solutions around 6.9 MHz. Three different models with different degrees of geometry simplifications were applied: simulations with the entire channel system (including the branched inlet/outlet), only the straight center channel, and the expansion chamber alone (see Fig. 1a). Except for the first model, the channel ends have been set to acoustically soft ends (open ends kept at ambient pressure) and the remaining boundaries to hard, perfectly reflecting walls. All simulations were performed for a maximum mesh size of 20 μm. This corresponds to approximately 10 mesh points per wavelength at the investigated frequencies in an aqueous medium.

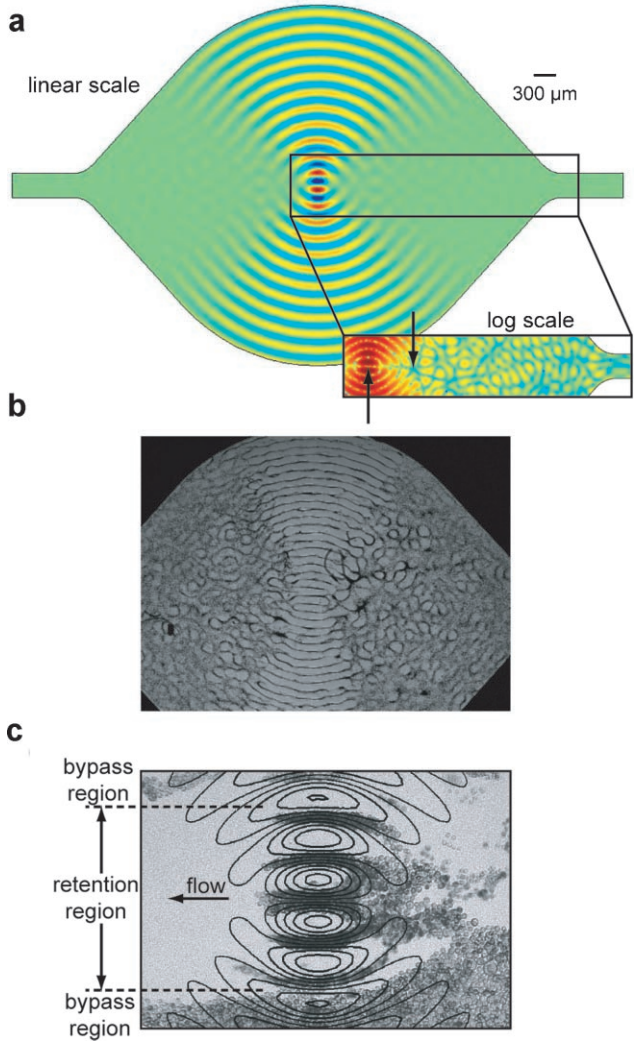

Figure 2. **a**: Theoretical modeling of the acoustic pressure field in the expansion chamber at 6.92 MHz. The arrows mark the observed trapping sites in Figure 3. **b**: No-flow experimental verification at 7.07 MHz. The micrograph shows the distribution of 5 μm beads (dark pattern) after 10 s of ultrasonic actuation without fluid flow. The acoustic forces are proportional to the square of the pressure field and tend to drive particles to the pressure nodes (green areas, in between yellow/red and turquoise/blue areas, in Fig. 2a). **c**: Flow-through experimental verification with COS-7 cells at 7.20 MHz. Contour lines from the simulated pressure field in (a) are superimposed to the micrograph.

Results

Resonance Characterization in the Expansion Chamber

The simulated and experimental particle responses to actuation of the expansion chamber during no-flow conditions are shown in Figure 2a and b, respectively. In Figure 2a, the simulated acoustic pressure field is shown for the eigenfrequency 6.92 MHz. The top-view, linear-scale, color plot displays high-pressure areas (red and blue in Fig. 2a) focused in the center of the chamber. The log-scale color plot (inset in Fig. 2a) reveals a non-zero fine structure on the upstream and downstream sides of the chamber center. The simulated field is verified in Figure 2b, where 5 μm polyamide beads are manipulated at 7.07 MHz during 10 s without fluid flow. The dark bead pattern displays areas with zero forces, proportional to the square of the acoustic pressure amplitude (Gröschl, 1998). The thin near-horizontal lines of packed beads above, below, and in the center of the chamber appear within less than 1 s and correspond well with the simulated linear-scale pressure pattern in Figure 2a. The more complex pattern outside the region of lines appears within 10 s and corresponds well with the simulated log-scale pattern in Figure 2a.

Figure 2c demonstrates flow-through operation of the chip at 7.20 MHz with a sample flow from right to left containing COS-7 cells. Here, contour lines from the

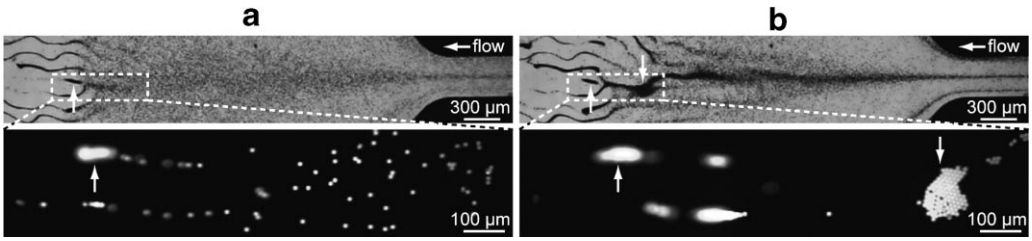

Figure 3. Characterization of the retention sites in the expansion chamber during fluid flow and 7.07 MHz actuation. The upper panels show manipulation of 5 μm beads, and the lower panels show manipulation of 10 μm fluorescent beads. The flow rates are 50 μL/min (**a**) and 2.5 μL/min (**b**). The arrows pointing up indicate the location of maximum retention forces where a 3D aggregate is trapped. The arrows pointing down indicate the location where a 2D aggregate is positioned and retained. The dashed rectangles indicate the scale and position of the micrographs in the lower panels relative to the micrographs in the upper panel.

modeled field in Figure 2a are superimposed on the micrograph. In the fit, the node-to-node distance of 120 μm was chosen. As seen in the image, the axial acoustic forces in the five central pressure nodes (marked with "retention region" in Figure 2c) are balanced with the viscous competing drag. The result is localized retention of the incoming COS-7 cells distributed within an area of size ~0.5 mm × 0.2 mm, while bypassing all other incoming cells in the peripheral nodes outside this retention region. At the present flow rate (1 μL/min), the axial retention force in the center of the chamber is approximately 10 pN for the COS-7 cells.

The retention performance is investigated in more detail in Figure 3. Here, the chamber is actuated at 7.07 MHz while slowly decreasing the flow rate. The upper panels show manipulation of 5 μm beads within a region corresponding to the black rectangle in Figure 2a, and the lower panels show manipulation of 10 μm fluorescent beads within a region corresponding to the dashed white boxes in the upper panels. The trapping and retention first start at the bead velocity of 3.0 mm/s at the location marked with an arrow pointing up in Figure 3a. Here, a 3D aggregate is formed very close to the mid-point of the chamber. The retention force on the first trapped 10 μm bead is 280 pN, and the corresponding fluid flow rate is 50 μL/min. When the bead velocity is decreased to 0.15 mm/s another trapping location (marked with an arrow pointing down in Fig. 3b) appears approximately 0.7 mm in the upstream direction from the first location. Here, a 2D aggregate is formed and levitated approximately 50 μm from the channel bottom. The retention force on the first trapped 10 μm bead is now 14 pN, and the corresponding fluid flow rate is 2.5 μL/min. The locations for 3D and 2D retention are also marked in the inset in Figure 2a with arrows pointing up and down, respectively. Thus, the levitation function, causing 2D aggregation, is restrained at the chamber center due to the dominating transverse (horizontal) forces. However, as demonstrated in Figure 3b, 2D retention can be accomplished at slightly lower flow rates and will be investigated in more detail in the next section.

Finally, it should be noted that while the theoretical simulations can be used to predict the overall shape of the force field in the microfluidic system (cf. Fig. 2), it is more difficult to accurately predict the resonance frequency. Frequency difference between experimental and simulated modes has previously been observed and discussed (Hagsäter et al., 2007, 2008; Manneberg et al., 2008a), and is an artifact from the simplified boundary conditions of the model that only take into account the fluid channel and not its supporting solid structures of the chip. In practice, several experimental chamber resonances similar to the modeled resonance in Figure 2a exist, for example, at 6.87, 7.07 (in Figs. 3 and 4), 7.20 (in Fig. 2c), and 7.84 MHz. In our present setup, the 7.07-MHz resonance seems to generate the strongest forces.

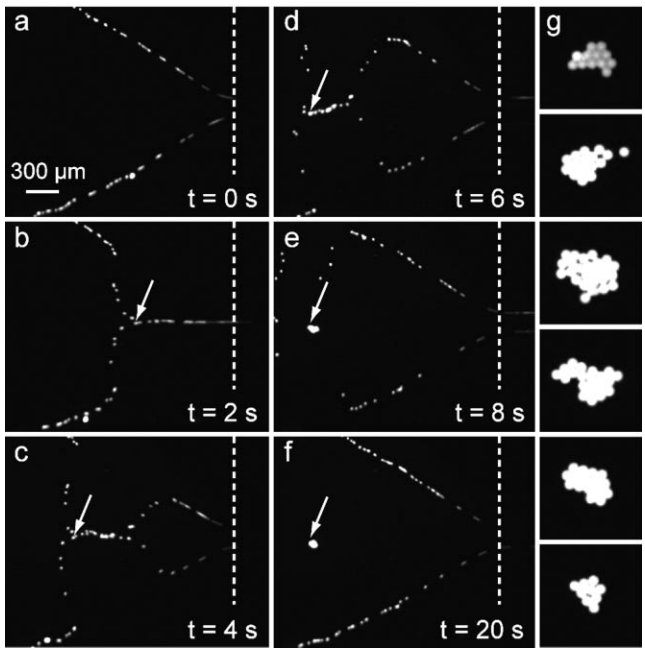

Figure 4. Demonstration of selective retention and positioning from a continuous sample flow (5 μL/min) containing 10 μm fluorescent beads: sample bypass (**a**), sample injection (**b**), sample bypass (**c**), and sample aggregation and retention (**d**–**f**). The actuation frequencies are 4.60 and 7.07 MHz in (a) and (c–f), and 2.13 and 7.07 MHz in (b). **g**: The retention result of six consecutive 1-s long injections.

Sample Selection, Retention, and Positioning

In this section, we will demonstrate how to select, retain, and position a discrete subpopulation of cells or particles from a continuous sample flow, according to the scheme presented in Figure 1c. Here, the chip is actuated by three transducers operating around 2.1, 4.6, and 6.9 MHz (cf. Fig. 1a).

Figures 4a–f are frames from a video sequence when the chip is operated at a constant sample flow rate of 5 μL/min. The dashed vertical line indicates the end of pre-alignment channel (right side) and the beginning of the expansion chamber (left side). The sample is 10 μm fluorescent beads suspended in water to a concentration of $\sim 10^5$ mL^{-1}. During the whole sequence, the expansion chamber is continuously actuated at 7.07 MHz. The process begins with pre-alignment of particles (on the right side of the vertical dashed line) into two nodes at 4.60 MHz actuation, resulting in bypassing of particles through peripheral streamlines in the expansion chamber (cf. Fig. 4a). Then, by switching to 2.13 MHz actuation, particles in the pre-alignment channel are aligned into a single node, which is used for injection of particles into a streamline crossing the center of the expansion chamber (cf. Fig. 4b). When switching back to 4.60 MHz actuation, all particles still present in the pre-alignment channel are bypassed when they enter the expansion chamber (cf. Fig. 4c). Thus, only the particles passing the vertical dashed line in Figure 4 during the 3-s long time interval between switching from 4.60 to 2.13 and back to 4.60 MHz are injected towards the retention region. Finally, the injected particles are trapped, aggregated, and retained close to the center of the expansion chamber (cf. Fig. 4d–f).

The white arrows in Figure 4b–f track a single particle through the selection and trapping process. For this choice of flow rate and particle concentration, the time scale for the whole process is less than 10 s. The 3-s long injection in Figure 4b resulted in 31 selected and positioned beads. The result of repeated 1-s injections are displayed in Figure 4g. As seen in the micrographs, the beads are closely packed in horizontal monolayers, which are levitated and positioned in between the channel floor and roof. For the six injections, the number of collected and retained beads is 16.5 ± 6.0 (average and standard deviation). If we assume that the individual bead injection events are uncorrelated, we would expect a Poisson distribution of the counting statistics, that is, $N \pm \sqrt{N}$. The observed counting statistics is in agreement with this hypothesis. Single-particle injection accuracy can in principle be obtained at low particle concentrations and flow rates, followed by manual switching between the pre-alignment frequencies. However, under such circumstances the collection efficiency is of the order of a few particles per minute. It should also be noted that a retained aggregate with 10 or more particles or cells can be retained in the chamber for several hours during constant-flow medium perfusion. The only observed perturbation source causing unwanted release of trapped particles is the occurrence of air bubbles in the fluid channel. Such problems are typically related to the external pump and tubing system connected to the chip.

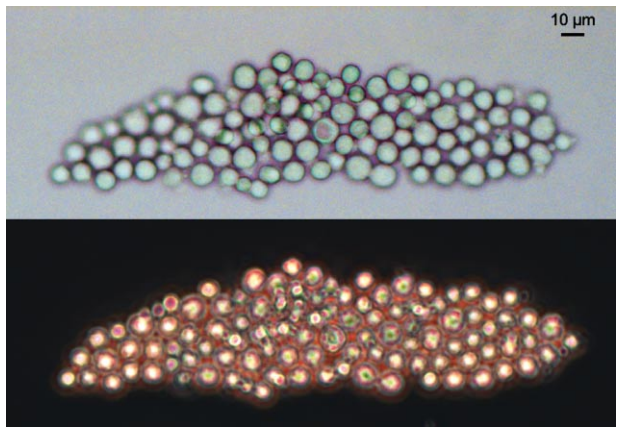

Figure 5. Label-free transillumination imaging of positioned and retained COS-7 cells in the expansion chamber, visualized by phase-contrast (top panel) and dark-field (bottom panel) microscopy. [Color figure can be seen in the online version of this article, available at www.interscience.wiley.com.]

Optical Characterization of Cells

Since the retained cell aggregate can be positioned and arranged as a horizontal monolayer (cf. Fig. 4g), we may perform cell characterization based on high-resolution microscopic monitoring, as previously demonstrated with fluorescent labels in Manneberg et al. (2008b). In Figure 5, we demonstrate examples of label-free imaging of an ultrasonically retained aggregate containing ~100 COS-7 cells using transillumination techniques: phase-contrast and dark-field microscopy. Thus, the device is compatible with both functionality studies based on, for example, fluorescent probes, as well as with label-free studies, for example, the morphology or topology of cells.

Discussion

In this section, we exemplify and discuss different target applications that our device is designed for. We have identified two different potential bio-applications, where the chip will be operated in slightly different functional modes: (I) Ultrasensitive bead-based biomolecular detection and (II) serial screening and/or long-term characterization of cells. The presented results in the former section are proof of concepts of the below applications.

In the first application (I), the chip can be used for ultrasonic enhancement of bead-based immunoassays (Wiklund et al., 2004) incubated at ambient analyte conditions (Ekins, 1989). Basically, the trick to obtain high sensitivity is to incubate the sample with extremely diluted bead-based

reagents (Wiklund and Hertz, 2006a). The ultrasound is then used for bead enrichment and positioning followed by confocal fluorescence detection. While the current device is built on a 96-well plate platform and suffers from limitations in both the optical detection performance and the enrichment efficiency (Wiklund et al., 2004), our chip-based platform presented in this study has potential to significantly improve both these factors. Since the aim is to enrich and position all incoming beads in a monolayer in the detection zone (the center of the expansion chamber), we only need the manipulation functions pre-alignment/injection and retention/positioning, and not the selection/bypassing functions (see Fig. 4).

In the second application (II), the set of manipulation functions demonstrated in Figure 4 (i.e., bypass—injection—retention—positioning—bypass) can be used repeatedly for real-time investigation of the cellular response to variations in a particular parameter of interest (e.g., concentration of a chemical compound or biomolecule). With our presented device, it is possible to assemble and position a small aggregate of 10–100 cells within ~10 s, followed by optical monitoring while bypassing excess cells from a continuously feeding sample flow. Thus, after a cell aggregate has been assembled and positioned, the bypass function prevents delayed addition of cells to the aggregate. This is important for defining a starting time valid for all cells in the aggregate when monitoring time-dependent biological processes. Furthermore, since ultrasonic cell handling is a gentle and biocompatible method (Bazou et al., 2005; Evander et al., 2007; Hultström et al., 2007; Svennebring et al., 2007), it is also possible to study the dynamics of a cellular parameter during long terms (hours to days). Examples of such "slow" parameters are monitoring of activation, differentiation and proliferation processes of individual cells. Future planned applications include dynamic monitoring of immunological synapses for studying immune cell interactions (Davis and Dustin, 2004).

The authors gratefully thank Prof. Hans M. Hertz for valuable discussions. This study was generated in the context of the *CellPROM* project, funded under the 6th Framework Program of the European Community (Contract No. NMP4-CT-2004-500039). The work was also supported by the Swedish Research Council for Engineering Sciences and the Göran Gustavsson Foundation.

References

Bazou D, Kuznetsova LA, Coakley WT. 2005. Physical environment of 2-D animal cell aggregates formed in a short-pathlength ultrasound standing wave trap. Ultrasound Med Biol 31:423–430.

Brandt EH. 1989. Levitation in physics. Science 243:349–355.

Davis DM, Dustin ML. 2004. What is the importance of the immunological synapse? Trends Immunol 25:323–327.

Ekins RP. 1989. Multi-analyte immunoassay. J Pharm Biomed Anal 7: 155–168.

Evander M, Johansson L, Lilliehorn T, Piskur J, Lindvall M, Johansson S, Almqvist M, Laurell T, Nilsson J. 2007. Noninvasive acoustic cell trapping in a microfluidic perfusion system for online bioassays. Anal Chem 79:2984–2991.

Gröschl M. 1998. Ultrasonic separation of suspended particles—Part I: Fundamentals. Acta Acustica 84:432–447.

Haake A, Neild A, Radziwill G, Dual J. 2005. Positioning, displacement, and localization of cells using ultrasonic forces. Biotechnol Bioeng 92:8–14.

Hagsäter SM, Glasdam Jensen T, Bruus H, Kutter JP. 2007. Acoustic resonances in microfluidic chips: Full-image micro-PIV experiments and numerical simulations. Lab Chip 7:1336–1344.

Hagsäter SM, Lenshof A, Skafte-Pedersen P, Kutter JP, Laurell T, Bruus H. 2008. Acoustic resonances in straight microchannels: Beyond the 1D-approximation. Lab Chip 8:1178–1184.

Harris NR, Hill M, Beeby S, Shen Y, White NM, Hawkes JJ, Coakley WT. 2003. A silicon microfluidic ultrasonic separator. Sensors Actuators B 95:425–434.

Hawkes JJ, Barber RW, Emerson DR, Coakley WT. 2004. Continuous cell washing and mixing driven by an ultrasound standing wave within a microfluidic channel. Lab Chip 4:446–452.

Hertz HM. 1995. Standing-wave acoustic trap for nonintrusive positioning of microparticles. J Appl Phys 78:4845–4849.

Hultström J, Manneberg O, Dopf K, Hertz HM, Brismar H, Wiklund M. 2007. Proliferation and viability of adherent cells manipulated by standing-wave ultrasound in a microfluidic chip. Ultrasound Med Biol 33:145–151.

Laurell T, Petersson F, Nilsson A. 2007. Chip integrated strategies for acoustic separation and manipulation of cells and particles. Chem Soc Rev 36:492–506.

Lilliehorn T, Simu U, Nilsson M, Almqvist M, Stepinski T, Laurell T, Nilsson J, Johansson S. 2004. Trapping of microparticles in the near field of an ultrasonic transducer. Ultrasonics 43:293–303.

Lilliehorn T, Nilsson M, Simu U, Johansson S, Almqvist M, Nilsson J, Laurell T. 2005. Dynamic arraying of microbeads for bioassays in microfluidic channels. Sensors Actuators B 106:851–858.

Manneberg O, Hagsäter SM, Svennebring J, Hertz HM, Kutter JP, Bruus H, Wiklund M. 2009. Spatial confinement of ultrasonic force fields in microfluidic channels. Ultrasonics 49:112–119.

Manneberg O, Svennebring J, Hertz HM, Wiklund M. 2008a. Wedge transducer design for two-dimensional ultrasonic manipulation in a microfluidic chip. J Micromech Microeng 18: 095025 (9pp).

Manneberg O, Vanherberghen B, Svennebring J, Hertz HM, Önfelt B, Wiklund M. 2008b. A three-dimensional ultrasonic cage for characterization of individual cells. Appl Phys Lett 93: 063901 (3pp).

Nilsson A, Petersson F, Jönsson H, Laurell T. 2004. Acoustic control of suspended particles in micro fluidic chips. Lab Chip 4:131–135.

Petersson F, Nilsson A, Jönsson H, Laurell T. 2005. Carrier medium exchange through ultrasonic particle switching in microfluidic channels. Anal Chem 77:1216–1221.

Petersson F, Åberg L, Swärd-Nilsson A-M, Laurell T. 2007. Free flow acoustophoresis (FFA)—A new microfluidic based mode of particle and cell separation. Anal Chem 79:5117–5123.

Svennebring J, Manneberg O, Wiklund M. 2007. Temperature regulation during ultrasonic manipulation for long-term cell handling in a microfluidic chip. J Micromech Microeng 17:2469–2474.

Wiklund M, Hertz HM. 2006a. Ultrasonic enhancement of bead-based bioaffinity assays. Lab Chip 6:1279–1292.

Wiklund M, Nilsson S, Hertz HM. 2001. Ultrasonic trapping in capillaries for trace-amount biomedical analysis. J Appl Phys 90:421–426.

Wiklund M, Toivonen J, Tirri M, Hänninen P, Hertz HM. 2004. Ultrasonic enrichment of microspheres for ultrasensitive biomedical analysis in confocal laser-scanning fluorescence detection. J Appl Phys 96:1242–1248.

Wiklund M, Günther C, Lemor R, Jäger M, Fuhr G, Hertz HM. 2006b. Ultrasonic standing wave manipulation technology integrated into a dielectrophoretic chip. Lab Chip 6:1537–1544.

Xie WJ, Wei B. 2001. Parametric study of single-axis acoustic levitation. Appl Phys Lett 79:881–883.